GEOSTANDARDS and GEOANALYTICAL RESEARCH

Chemical analysis of iron meteorites by field-portable X-ray fluorescence.

Journal:	*Geostandards and Geoanalytical Research*
Manuscript ID:	GGR-0291.R2
Manuscript Type:	Original Article
Date Submitted by the Author:	n/a
Complete List of Authors:	Gemelli, Maurizio; Università di Pisa, Dipartimento di Scienze della Terra D'Orazio, Massimo; Università di Pisa, Dipartimento di Scienze della Terra Folco, Luigi; Università di Pisa, Dipartimento di Scienze della Terra
Keywords:	field-portable X-ray fluorescence, iron meteorites, bulk composition, classification, cosmochemistry

Title

Chemical analysis of iron meteorites by hand-held X-ray fluorescence.

Authors

Maurizio **Gemelli***, Massimo **D'Orazio**, Luigi **Folco**

Affiliation

Addresses: Dipartimento di Scienze della Terra, Università di Pisa, Via S. Maria 53, I-56126 Pisa, Italy

E-mail addresses:

*corresponding author: gemelli@dst.unipi.it

Massimo D'Orazio: massimo.dorazio@unipi.it

Luigi Folco: luigi.folco@unipi.it

Phone number: +390502215796

Fax number: +390502215800

Abstract

We evaluate the performance of a hand-held XRF (HHXRF) spectrometer in the bulk analysis of iron meteorites. Analytical precision and accuracy were tested on CRMs metal alloys and iron meteorites of known chemical composition. With minimal sample preparation (i.e., flat and roughly polished) HHXRF allows the accurate and precise ~~analysis~~ determination of most elements heavier than Mg with concentrations greater than 0.01 % m/m in CRM metal alloys, and of major elements Fe and Ni and minor elements Co, P and S (generally ranging from 0.1

to 1 % m/m) in iron meteorites. In addition, multiple HHXRF spot analyses can be used to determine the bulk chemical composition of iron meteorites, which are often characterized by sulphides and phosphides accessory minerals. In particular, it is possible to estimate the P and S bulk contents, which are of critical importance for the petrogenesis and evolution of Fe-Ni rich liquids and iron meteorites. This study thus validates HHXRF as a valuable tool for use in meteoritics, allowing the rapid, non-destructive: 1) identification of the extraterrestrial origin of metallic objects (i.e., archaeological artefacts); 2) preliminary chemical classification of iron meteorites; 3) identification of mislabelled/unlabelled specimens in museums and private collections; 4) bulk analysis of iron meteorites.

Keywords

Hand-held XRF, iron meteorites, bulk composition, cosmochemistry

Introduction

Since the first archaeological and geological applications in the 1960s (Shackley 2011), X-ray fluorescence (XRF) has become one of the most commonly used analytical techniques for determining the chemical composition of a variety of materials. The recently developed hand-held XRF units (HHXRF) have been used for numerous applications in the field. These applications include the ~~analysis~~ determination of metals in soils (Kalnicky and Singhvi 2001, Radu and Diamond 2009) and sediments (Kenna *et al*. 2011, Kirtay *et al.* 1998), analysis of artefacts and artworks (Liritzis and Zacharias 2011, Vázquez *et al.* 2012), quality tests in metallurgical industry and engineering, identification and classification of hazardous wastes (Vanhoof *et al.* 2013). The reasons for the significant success of HHXRF (Potts and West 2009) include i) portability of the instrument, ii) the easy handling of the operating system, iii) minimal sample preparation iv) rapid, non-destructive field analyses with remarkable reproducibility and low detection limits for elements heavier than Mg.

The XRF technique has been widely used for the bulk chemical analysis of meteorites since the late 1960s and early 1970s (i.e., Reed 1972). More recently, HHXRF was used for the first time to identify and classify different groups of stony meteorites, and to quantify their terrestrial elemental contamination (Zurfluh *et al.* 2011). In this work we tested a commercial HHXRF instrument for its suitability in the bulk chemical analyses of iron meteorites, encouraged by the fact that HHXRF was designed mainly for the metallurgical and mining industry, especially for the analysis of metal alloys.

Iron meteorites are made of Fe-Ni metal alloys of asteroidal origin containing minor amounts of Co, P and S and trace amounts of siderophile (Ga, Ge, Ir, Au, Pt, Pd, Mo, W, Rh, Ru) and chalcophile (Cu, Zn, As, Ag) elements in highly variable concentrations (differing by up to five orders of magnitude). The Ni content varies from ~ 4 to 60 % m/m, although it most commonly ranges from 5 to 12 % m/m. The chemical classification and petrogenesis of iron meteorites is based on siderophile trace element concentrations (i.e., Ir, Ge, Ga, Au) (i.e., Goldstein *et al.* 2009). Due to their low abundances (typically of the order of 10^{-4} to 10^{3} µg g^{-1}), their concentrations are determined by means of sensitive analytical methods like INAA and radiochemical (RNAA) neutron-activation analysis (Wasson *et al.* 1989) or ICP-MS (D'Orazio and Folco 2003). In the following sections we illustrate the analytical precision and accuracy of a NITON XL3t GOLDD+ hand-held spectrometer in the analyses of a representative set of iron meteorites. We also discuss the advantages and limitations of using this rapid, non-destructive and practical analytical method in meteoritics, namely, in the identification, classification and geochemical analysis of iron meteorites.

Method and samples

The instrument

The instrument used in this study is a NITON XL3t GOLDD+ XRF spectrometer. It is equipped with a miniaturized tube with an Ag anode (50 kV, 200 µA, 2 W). The instrument is

fitted with an SDD detector capable of acquiring spectra at high count rates. Accordingly, the instrument is equipped with an X-ray tube capable of operating at higher outputs compared to instruments fitted with a Si(PIN) detector. ~~High currents are possible because the XL3t GOLDD+ analyser can process a higher rate of X-ray counts and high-count rates can increase precision (i.e., repeatability) and/or decrease analytical time. The XL3t GOLDD+ analyser is equipped with a silicon drift detector (SDD).~~ Different measuring modes are available: 'Soil', 'Mining', and 'General Metals'. We exclusively used the 'General Metals' mode for this study because is more suitable for our sample types. This procedure allowed the simultaneous detection of over 18 elements (see Table 1), including those of interest in the analysis of iron meteorites (Fe, Ni, Co, P, S, Cr, Cu, W and Mn). In this mode the instrument works in different conditions in order to optimize analysis: 'main' (excitation 50 kV, 40 µA), 'low' (15 kV, 133 µA) and 'light' (8 kV, 200 µA). Limit of detection (LOD) for each analyte was calculated as three times the standard deviation of the concentration measured in samples with none or only a trace amount of the analyte.

The list of elements measured and operative conditions are shown in Table 1. The counting times for the three different operative modes was 60s each, making a total acquisition time of 180s for a single analysis. The on-board software for the XL3t uses a 'Fundamental Parameters' correction algorithm that involves iterative corrections to the measured X-ray counts on the basis of the approximated compositions, accounting for differences in X-ray emission, absorption, secondary fluorescence and other phenomena. The analyses were performed with the device mounted on a stand with a shielded box protecting the user from radiation. Samples were positioned accurately in the analytical plane of the XRF instrument and no additional corrections for air gap were required. The beam diameter of this specific instrument is ~ 8 mm, but it can be reduced to 3 mm using a built-in spot collimator. The spectra of the measurements were transferred on a computer using the Niton Data Transfer software.

Standard samples

In order to define the optimal analytical conditions and verify the quality of the analytical procedure on metals, we selected a set of steel CRMs which were analysed in each analytical session. Selected CRMs are iron-nickel alloys with composition similar to iron meteorites to match matrix effects. They are in the form of thin cylinders with flat basal surfaces which are physically similar to the flat surfaces of the analysed iron meteorites (see below). They included the certified NIST reference steels SRM 1262b and SRM 1158, and the Analytical Reference Materials International (ARMI) steels 35JN and AISI 303 (Table 2).

Iron meteorite samples

Iron meteorites are made of Fe-Ni metal phases (mostly kamacite and taenite, secondarily tetrataenite, martensite, awaruite) plus accessory sulphides (i.e., troilite, daubreelite), phosphides (i.e., schreibersite), nitrides (i.e., carlsbergite), carbides (i.e., cohenite), oxides (i.e., chromite) and phosphates (i.e., farringtonite), and sometimes by substantial amounts of silicate inclusions (Mittlefehldt D.W. 1998). More than about 99.5 % m/m of the metallic portion of iron meteorites consists of Fe, Ni and Co, while the remaining mass is made of siderophile and chalcophile trace elements showing a highly variable relative distribution (up to over a factor of 10^5). Structurally, iron meteorites are classified in octahedrites, ataxites and hexahedrites. Octahedrites consist of kamacite lamellae oriented along octahedral planes separated by Ni-rich lamellae composed of several phases. This structure, particularly evident on polished and etched surfaces, is known as the Widmanstätten pattern (Figure 1). Octahedrites are further subdivided according to the width of the kamacite lamellae, from coarsest (> 3.3 mm) to finest (< 0.2 mm). Ataxites show only microscopic spindles of kamacite. Hexahedrites consist almost entirely of kamacite, with their name referring to the cleavage of this mineral phase. While the structural subdivision is purely descriptive, a genetically more significant classification is based on the Ni and trace element content of the metal phase, particularly Ga, Ge and Ir. The concentration of Ni, the second most abundant

element in iron meteorites after Fe, must be known in order to interpret the structure of iron meteorites based on the sub-solidus portion of the Fe-Ni phase diagram (Yang and Goldstein 2005). At present, thirteen chemical groups (IAB, IC, IIAB, IIC, IID, IIE, IIF, IIG, IIIAB, IIIE, IIIF, IVA, IVB) have been distinguished (Wasson *et al.* 1998 and references therein), with the Roman numerals I to IV indicating decreasing contents of Ga and Ge. Each group is composed of at least five distinct meteorites. Iron meteorites that do not fall in any of these chemical groups (about 16%) are called "ungrouped", whereas irons in which concentrations of only one or two elements fall outside the typical range of a specific group are called "anomalous". The study of the structure, chemistry and isotopic composition of iron meteorites is fundamental for understanding the process of planetary differentiation (including that of the proto-Earth) and the chemical evolution of the Solar System (i.e., Goldstein et al. 2009).

HHXRF analyses were conducted on a set of fifteen iron meteorites and the metal fraction of a Main Group Pallasite of well-known chemical composition (Table 2). We selected samples with a good compositional variability in order to be representative of the different chemical and structural classes, i.e. from coarsest octahedrites to ataxites with Ni contents ranging from ~ 5 to 32 % m/m (see Table 4).

Bulk chemical composition analyses were carried out on interior ground surfaces (600 mesh) of meteorite slabs (Figure 1) or end cuts. This minimal specimen preparation, which is the customary approach used by researchers or dealers to start characterizing new iron meteorites, is enough for quantitative X-ray analyses to minimize- inconsistencies caused by small variations in the surface-to-instrument distance and~~undesirable~~ random unaccounted absorption due to the roughness of the surface.

To avoid surface contamination, all samples were washed in an ultrasonic bath with acetone and then allowed to dry prior to analyses. Care was taken to analyse surfaces devoid of accessory minerals visible to the naked eye, in order to obtain the actual metal phase composition, which is the composition used for the chemical classification of iron meteorites. The number of spot analyses on each iron meteorite increased with increasing mineralogical

heterogeneity of the specimen in order to better approximate the representativeness of the analyses. For instance, the number of spot analyses were typically <10 for homogeneous samples like some ataxites (i.e., Figure 1f), between 10 and 20 for samples showing some heterogeneity of the metal phase at the scale of the analysed surfaces, like the coarse octahedrites (Figure 1b,c). Gridded spot analyses of Gebel Kamil were conducted to assess the capability of HHXRF in determining the bulk meteorite composition (i.e., metal plus accessory minerals) of heterogeneous irons characterized by scattered mm-sized sulphide and phosphide crystals (Figure 1e). Lastly, we performed HHXRF analyses on the external surface of the latter meteorite to show how this method can be used for the rough identification of an iron meteorite in case an internal, flat and polished surface could not be available, as it may happen in the field during its finding.

Results

HHXRF compositional data of CRMs are presented in Table 3. In Figure 2 they are plotted against reference values. HHXRF data show a nearly one-to-one relationship across a broad range of elemental compositions. Relatively larger deviations are observed only for those elements present in very low concentrations (< 0.1 % m/m). RSD% varies from ~ 10 to 20 for P, S, V, Sn, Sb. Furthermore, analyses of CRMs were performed over seven months using the same analytical procedure and setting to check the long-term precision of the instrument. Results indicate a very good stability over time for several elements with RSD% ranging between 1 and 5 (Figure 3).

The HHXRF bulk metal composition of fifteen iron meteorites obtained from the analyses of cut surfaces is listed in Table 4, along with standard deviation, RSD% for each sample and reference values from literature. The match is good and the RSD% varies from less than 1 to 5 for the most abundant elements, i.e., Fe, Ni and Co. Figure 4 shows HHXRF measurements plotted against reference data. The best results were obtained for Fe, Ni and Co, which are the most abundant elements in iron meteorites. The relatively large deviations for some elements

such as Cr and Cu are possibly due to the very low concentrations of these elements close to the limit of detection (i.e., 450 μg g^{-1} for Cu and 80 μg g^{-1} for Cr (Table 5). Poor correlations of P and S in Campo del Cielo, Canyon Diablo and North Chile meteorites are related to weak reference values which were derived through modal estimation models (Buchwald 1975).

One of the major problems in the determination of the bulk composition of iron meteorites may be their compositional heterogeneity, determined by the size and spatial distribution of the constituent phases (i.e., the kamacite-taenite intergrowths, accessory minerals, etc.; Figure 1), relative to the size of the X-ray beam. We thus focused on the systematic analysis of a highly heterogeneous meteorite at the specimen scale in order to assess how many HHXRF spot analyses are required to obtain a representative bulk chemical composition that takes into account the occurrence of mm-sized crystals (or larger). For this purpose, we selected Gebel Kamil, a recently classified iron meteorite (D'Orazio *et al.* 2011) from Egypt, which has millimetre-sized troilite (FeS), schreibersite ($[Fe,Ni]_3P$) and daubreelite ($[Fe,Cr]_2S_4$) crystals in a cm-scale spacing arrangement (Figure 1). We performed 166 HHXRF spot analyses on numerous meteorite slabs adopting an 8 mm spot and a grid spacing of 1 cm for a total of 83.4 cm^2 of analysed surface. The dynamic average of the concentrations of Fe, Ni, S, P and Co (i.e., the variations of the average values of the concentrations of these elements with increasing number of analyses) is plotted in Figure 5. The plot reveals significant offsets and systematic divergences associated to the occasional analyses of mm-sized sulphide and phosphide crystals. Note in fact that each positive spike of P and S coincides with a negative spike of Ni and Fe. Overall, these divergences reflect the different P, S and Fe, Ni ratios of the mm-sized phosphide and sulphide crystals and host metal. As expected, after an initial scattering, data tend to stabilize around constant values, and ~ 3x differences in the P and S bulk contents are observed relative to the metal composition (Table 4). Furthermore examining HHXRF bulk meteorite analysis of Gebel Kamil (SMTable 1) it is possible to count the same number of visible phosphide and sulphide crystals and then to estimate a ~ 1:1 ratio between phosphide and sulphides that is different from that estimated by D'Orazio *et al.* 2011.

The HHXRF analysis of the external surface of Gebel Kamil is given in Table 6. The analysis reveals a lower Fe/Ni (3.2) ratios relative to bulk metal and bulk meteorite compositions (3.8) from interior surfaces, and the occurrence of considerable Si, Al, S up to 9.1, 3.8 and 1.8 % m/m, respectively.

Discussion

Results suggest that the HHXRF employed in this study yields accurate and precise analyses of metal alloys for most elements heavier than Mg with minimum concentrations of 0.01 % m/m, as documented by CRMs analyses (Table 3). In addition, the instrument shows very good stability, as revealed by CRMs analyses over a seven months period (Figure 3). HHXRF is very effective in the quantification of elements in iron meteorites, especially major elements such as Fe, Ni and minor elements such as Co, P and S, which generally range from 0.1 to 1 % m/m. This is documented by the good agreement between HHXRF data from cut (and roughly polished) surfaces of the analysed iron meteorites and reference data from literature (Figure 4). As a result, HHXRF analyses allow discrimination of different iron meteorites.

HHXRF analyses of cut surfaces can also be used to constrain the classification of iron meteorites. Figure 6 shows the Ni vs. Co diagram of the iron meteorites analysed in this work by HHXRF relative to the major iron meteorite groups from literature. The analysed meteorites plot in the compositional fields of their respective chemical groups (Table 2). When coupled with petrographic and textural analysis, this information can be used to assign unknown iron meteorites to a limited number of chemical (and structural) classes.

The bulk P and S concentrations determined by ~~The capability of~~ HHXRF are adequate, in terms of precision and accuracy, to study~~to measure the bulk P and S contents in iron meteorites with good precision is a further advantage to study~~ the chemical evolution and petrogenesis of~~in~~ iron meteorite~~s petrogenesis~~. Note that the concentration of non-metal elements such as P, S and C determines the solidification behaviour and the distribution of

major, minor, and trace elements in iron meteorites (Goldstein *et al.* 2009). Furthermore, the amount of P present in the metal greatly influences the nucleation temperature, the reaction process, and the diffusion rate of Ni as the Widmanstätten pattern develops. The identified importance of P in the nucleation and growth of the Widmanstätten pattern has allowed to the development of new and more sophisticated models for the determination of cooling rates of iron meteorites (Goldstein *et al.* 2009). Since P and S are preferentially contained in accessory phases such as sulphides and phosphides, their size and distribution in the meteorite must be carefully assessed in order to select an appropriate analytical method for determining its bulk composition. According to the analytical protocol for INAA and ICP-MS analyses of iron meteorites, the metal sample must not contain visible inclusions and sulphide and phosphide crystals. The true meteorite bulk composition could be obtained by either dissolving a sample large enough to be representative, namely hundred grams of meteorite (or much more), or by integrating INAA or ICP-MS data with the geochemical contribution of the mm-sized accessory minerals obtained by modal analyses plus mineral chemistry (Buchwald 1975, Wasson *et al.* 2007). The first approach usually requires the destruction of large amounts of precious material and is often avoided; the second approach is often favoured, but can be inaccurate. In the case of meteorites containing large accessory minerals relative to the spot analysis, HHXRF is a suitable tool for determining bulk meteorite composition, including P and S. A comparison between HHXRF bulk metal composition and bulk meteorite composition of Gebel Kamil is given in Table 6. The 3x differences in P and S contents highlight the geochemical contribution of the mm-sized sulphide and phosphide crystals to the bulk meteorite composition and the usefulness of the method.

The comparison of the bulk compositions obtained by the HHXRF analyses of the interior and external surfaces of Gebel Kamil (Table 6) shows that HHXRF not only enables detection of the extraterrestrial signature of iron meteorites, namely the combination of major elements Fe, Ni and Co, but also the detection of their alteration in the terrestrial environment due to ablative flight, weathering and contamination. For instance, in the specific case of the Gebel Kamil shrapnel (i.e., a meteorite fragment devoid of fusion crust that formed upon

hypervelocity impact), the lower Fe/Ni is likely due to oxidation during weathering. The high concentrations of S, Si and Al are due contamination from the Sahara desert were it was found (Folco *et al.* 2010), most likely desert varnish (i.e., Lee and Bland 2003, Giorgetti and Baroni 2007).

Furthermore, since Fe, Ni and Co, along with P and S, are the most abundant diagnostic elements in iron meteorites, HHXRF can be used as a first analytical approach to distinguish extraterrestrial iron from iron artefacts. This is relevant as many valuable archaeological artefacts are made of meteoritic iron, as recently documented (i.e., Buchner *et al.* 2012; Johnson *et al.* 2013). Likewise, HHXRF can be used to identify paired specimens in meteorite collections, i.e., from dense meteorite collection areas, or mislabelled specimens in museum meteorite collections. The advantage of rapid, non-destructive methods in the curation of meteorites has already been demonstrated by Rochette *et al.* 2003, Rochette *et al.* 2008 and Folco *et al.* 2006 in the case of magnetic susceptibility measurements.

Conclusions

Analyses of CRMs and iron meteorites of known composition show that commercial HHXRF (NITON XL3t GOLDD+) allows accurate and precise determination of the concentrations of the major elements Fe and Ni, and the minor elements Co, P and S (generally ranging from 0.1 to 1% m/m) in iron meteorite metal. RSD% varies from less than 1 to 5 for the most abundant elements such as Fe, Ni and Co.

The procedure requires minimal sample preparation, i.e., flat, ground (≤ 600 Mesh) representative surfaces larger that the mm-sized X-ray spot size (3 or 8 mm in diameter in the XRF spectrometer used in this study). Analyses are rapid (180 s) and non-destructive.

Analyses of irregular external surfaces provide qualitative information about the extraterrestrial geochemical signature of iron meteorites, namely the detection of diagnostic

major and minor elements Fe, Ni, Co, P and S. They also provide information about their surface alteration in terrestrial environments due to ablative flight, weathering and contamination.

HHXRF thus proves to be a valuable and practical tool in meteoritics for curatorial purposes. It can be used to: i) confirm/verify the extraterrestrial origin of metallic objects; ii) complete the preliminary chemical classification of new iron meteorites; iii) identify mislabelled/unlabelled specimens in museums and private collections.

Multiple HHXRF spot analyses can be used to determine the bulk chemical composition of iron meteorites characterized by up to cm-sized crystals of accessory minerals with a mm- to cm-scale spacing (most commonly sulphides and phosphides). A test conducted on the heterogeneous Gebel Kamil iron meteorite, which is characterized by mm-sized and cm-spaced sulphide and phosphide crystals, required about 160 spot analyses (total analysed surface: 83 cm^2; total analysis time: ~ 8 hrs) to obtain a representative bulk meteorite composition for Fe, Ni, Co, P and S. Note that only few spot analyses are required for homogeneous meteorites like Hoba, Chinga, North Chile and Coahuila. Bulk P and S contents are of crucial petrological importance in modelling parent liquid evolution and subsolidus cooling rates. Their determination in a heterogeneous iron meteorite like Gebel Kamil by means of other customary methods like INAA and ICP-MS would require the destruction (digestion) of hundreds of grams of precious material.

Due to its main characteristics and capabilities (portability, and rapid, non-destructive, accurate analyses), HHXRF has great potential applications in archeometry, namely on-site identification and the examination and study of iron artefacts. It can be useful not only during archaeological excavations, but also when museums do not allow sampling of precious artefacts (as required for INAA or ICP-MS analysis) or even their temporary transfer to the laboratory.

Acknowledgements

This work was supported by the Italian Programma Nazionale delle Ricerche in Antartide, PNRA (project ID#: PEA2009, A2.08, Meteoriti Antartiche) and by the Italian Ministero degli Affari Esteri, Progetti di Grande Rilevanza 2013-2015, Protocollo Italia-Egitto (project ID#: PGR 00187, Geologia, geofisica e geocronologia del Kamil Crater, Egitto). M. Gemelli is also supported by the Italian Ministero dell'Istruzione, dell'Università e della Ricerca, MIUR "Futuro in Ricerca Programme 2013" (project ID#: RBFR13FIVO). We thank two anonymous referees for constructive review and the Associate Editor Prof. Thomas Meisel for editorial handling.

References

Benedix G.K., McCoy T.J., Keil K. and Love S.G. (2000)
A petrologic study of the IAB iron meteorites: Constraints on the formation of the IAB-Winonaite parent body. **Meteoritics & Planetary Science, 35,** 1127-1141.

Buchner E., Schmieder M., Kurat G., Brandstaetter F., Kramar U., Ntaflos T., Kroechert J. (2012)
Buddha from space—An ancient object of art made of a Chinga iron meteorite fragment. **Meteoritics & Planetary Science, 47**, 1491–1501.

Buchwald V.F. (1975)
Handbook of iron meteorites. **University of California Press (Berkeley USA),** 1-1416.

Choi B.-G., Ouyang X. and Wasson J.T. (1995)
Classification and origin of IAB and IIICD iron meteorites. **Geochimica et Cosmochimica Acta, 59,** 593-612.

D'Orazio M. and Folco L. (2003)
Chemical analysis of iron meteorites by Inductively Coupled Plasma-Mass Spectrometry. **Geostandards Newsletter, 27,** 215-225.

D'Orazio M., Folco L., Zeoli A. and Cordier C. (2011)
Gebel Kamil: The iron meteorite that formed the Kamil crater (Egypt). **Meteoritics & Planetary Science, 46,** 1179-1196.

Fazio A., D'Orazio M. and Folco L. (2013)
The extremely reduced silicate-bearing iron meteorite Northwest Africa 6583: implications on the variety of the impact melt rocks of the IAB-complex parent body. **Meteoritical & Planetary Science, 48,** 2451–2468.

Folco L., Di Martino M., El Barkooky A., D'Orazio M., Lethy A., Urbini S., Nicolosi I., Hafez M., Cordier C., van Ginneken M., Zeoli A., Radwan A.M., El Khrepy S., El Gabry M., Gomaa M., Barakat A.A., Serra R. and El Sharkawi M. (2010)
The Kamil Crater in Egypt. **Science, 329,** 804.

Folco L., Rochette P., Gattacceca J. and Perchiazzi N. (2006)
In situ identification, pairing, and classification of meteorites from Antarctica through magnetic susceptibility measurements. **Meteoritics & Planetary Science, 41,** 343-353.

Giorgetti G. and Baroni C. (2007)
High-resolution analysis of silica and sulphate-rich rock varnishes from Victoria Land (Antarctica). **European Journal of Mineraolgy, 19,** 381-389.

Goldstein J.I., Scott E.R.D. and Chabot N.L. (2009)
Iron meteorites: Crystallization, thermal history, parent bodies, and origin. **Chemie der Erde - Geochemistry, 69,** 293-325.

Jochum K.P., Seufert M., Begemann F. (1980)
On the distribution of major and trace elements between metal and phosphide phases of some iron meteorites. **Zeitschrift für Naturforschung, 35a,** 57-63.

Kalnicky D.J. and Singhvi R. (2001)
Field portable XRF analysis of environmental samples. **Journal of Hazardous Materials, 83,** 93-122.

Kenna T.C., Nitsche F.O., Herron M.M., Mailloux B.J., Peteet D., Sritrairat S., Sands E. and Baumgarten J. (2011)
Evaluation and calibration of a Field Portable X-Ray Fluorescence spectrometer for quantitative analysis of siliciclastic soils and sediments. **Journal of Analytical Atomic Spectrometry, 26,** 395-405.

Kirtay V.J., Kellum J.H. and Apitz S.E. (1998)
Field-portable X-ray Fluorescence Spectrometry for metals in marine sediments: Results from multiple sites. **Water Science and Technology, 37,** 141-148.

Johnson D., Tyldesley J., Lowe T., Withers P.J., Grady M.M. (2013)
Analysis of a prehistoric Egyptian iron bead with implications for the use and perception of meteorite iron in ancient Egypt. **Meteoritics & Planetary Science, 48**, 997-1006.

Lee M.R. and Bland P.A., (2003)
Dating climatic change in hot deserts using desert varnish on meteorite finds. **Earth and Planetary Science Letters, 206,** 187-198.

Liritzis I. and Zacharias N. (2011)
Portable XRF of Archaeological Artifacts: Current Research, Potentials and Limitations. **In: Shackley M.S. (ed), X-Ray Fluorescence Spectrometry (XRF) in Geoarchaeology. Springer New York,** 109-142.

Mittlefehldt D.W. T.J.M., Cyrena Anne Goodrich, and Alfred Kracher (1998)
Non-Chondritic Meteorites from Asteroidal Bodies. **In: Papike J.J. (ed), Planetary Materials (Reviews in Mineralogy),** 1-196.

Petaev M.I. and Jacobsen S.B., (2004)
Differentiation of metal-rich meteoritic parent bodies: I. Measurements of PGEs, Re, Mo, W, and Au in meteoritic Fe-Ni metal. **Meteoritics & Planetary Science, 39,** 1685–1697.

Potts P.J., West, M. (2009)
Portable X-ray fluorescence spectrometry-capabilities for in situ analysis. Edited by P. J. Potts and M. West. RSC Publishing, Cambridge, UK, 2008, 291 pp. ISBN 978 0 85404 552 5 **X-Ray Spectrometry, 38,** 157-157.

Radu T. and Diamond D. (2009)
Comparison of soil pollution concentrations determined using AAS and portable XRF techniques. **Journal of Hazardous Materials, 171,** 1168-1171.

Reed S.J.B. (1972)
Determination of Ni, Ga, and Ge in iron meteorites by X-ray fluorescence analysis. **Meteoritics, 7,** 257-262.

Rochette P., Sagnotti L., Bourot-Denise M., Consolmagno G., Folco L., Gattacceca J., Osete M.L. and Pesonen L. (2003)
Magnetic classification of stony meteorites: 1. Ordinary chondrites. **Meteoritics & Planetary Science, 38,** 251-268.

Rochette P., Gattacceca J., Bonal L., Bourot-Denise M., Chevrier V., Clerc J.-P., Consolmagno G., Folco L., Gounelle M., Kohout T., Pesonen L., Quirico E., Sagnotti L. and Skripnik A. (2008)
Magnetic classification of stony meteorites: 2. Non-ordinary chondrites. **Meteoritics & Planetary Science, 43,** 959-980.

Scott E.R.D. and Wasson J.T. (1976)
Chemical classification of iron meteorites—VIII. Groups IC. IIE, IIIF and 97 other irons. **Geochimica et Cosmochimica Acta, 40,** 103-115.

Shackley M.S. (2011)
An Introduction to X-Ray Fluorescence (XRF) Analysis in Archaeology. **In: Shackley M.S. (ed), X-Ray Fluorescence Spectrometry (XRF) in Geoarchaeology. Springer New York,** 7-44.

Vanhoof C., Holschbach-Bussian K.A., Bussian B.M., Cleven R. and Furtmann K. (2013)
Applicability of portable XRF systems for screening waste loads on hazardous substances as incoming inspection at waste handling plants. **X-Ray Spectrometry,** n/a-n/a.

Vázquez C., Palacios O., Lué-Merú M., Custo G., Ortiz M. and Murillo M. (2012)

Provenance study of obsidian samples by using portable and conventional X ray fluorescence spectrometers. Performance comparison of both instrumentations. **Journal of Radioanalytical and Nuclear Chemistry, 292,** 367-373.

Wasson J.T., Choi B.G., Jerde E.A. and Ulff-Moller F. (1998)
Chemical Classification of Iron Meteorites: XII. New Members of the Magmatic Groups - A newly identified pyroxene-bearing pallasite. **Geochimica et Cosmochimica Acta, 62,** 715-724.

Wasson J.T., Huber H. and Malvin D.J. (2007)
Formation of IIAB iron meteorites. **Geochimica et Cosmochimica Acta, 71,** 760-781.

Wasson J.T. and Ouyang X. (1990)
Compositional range in the Canyon Diablo meteoroid. **Geochimica et Cosmochimica Acta, 54,** 3175-3183.

Wasson J.T., Ouyang X., Wang J. and Eric J. (1989)
Chemical classification of iron meteorites: XI. Multi-element studies of 38 new irons and the high abundance of ungrouped irons from Antarctica. **Geochimica et Cosmochimica Acta, 53,** 735-744.

Wasson J.T. and Richardson J.W. (2001)
Fractionation trends among IVA iron meteorites: contrasts with IIIAB trends. **Geochimica et Cosmochimica Acta, 65,** 951-970.

Wlotzka F. and Jarosewich E. (1977)
Mineralogical and chemical compositions of silicate inclusions in the El Taco, Campo del Cielo, iron meteorite. **Smithsonian Contribution, Earth Sciences 19,** 104–125.

Yang J. and Goldstein J.I. (2005)
The formation of the Widmanstätten structure in meteorites. **Meteoritics & Planetary Science, 40,** 239-253.

Zurfluh F.J., Hofmann B.A., Gnos E. and Eggenberger U. (2011)
Evaluation of the utility of handheld XRF in meteoritics. **X-Ray Spectrometry, 40,** 449-463.

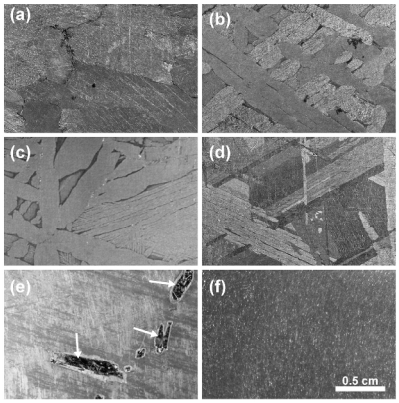

Figure 1. Stereomicroscopic images of polished and etched surface of six of the fifteen iron meteorites analysed by HHXRF in this work. All images were taken at the same magnification to better show relative heterogeneity in terms of texture and mineral composition. a) Campo del Cielo; coarse octahedrite; b) Canyon Diablo; coarse octahedrite; c) Seymchan, metal; coarse octahedrite; d) Muonionalusta; fine octahedrite; e) Gebel Kamil; ataxite; accessory mineral crystals (arrowed) consist of schreibersite, troilite and daubreelite; f) Chinga; ataxite.
297x420mm (300 x 300 DPI)

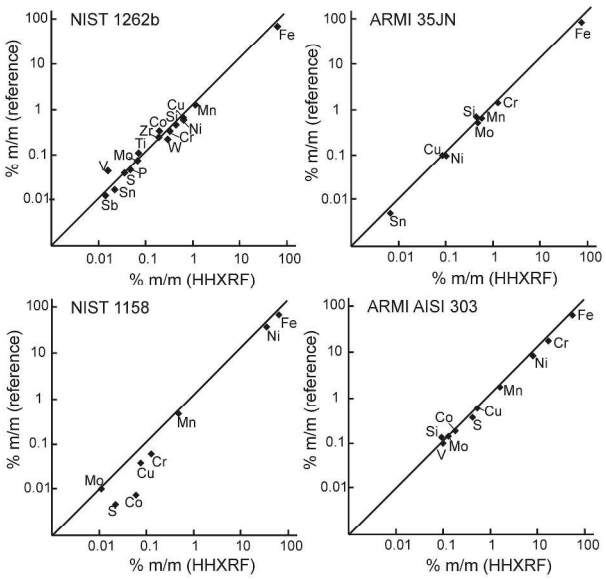

Figure 2. HHXRF elemental concentrations of CRMs plotted versus reference values. The line shows 1:1 linear correlation.
297x420mm (300 x 300 DPI)

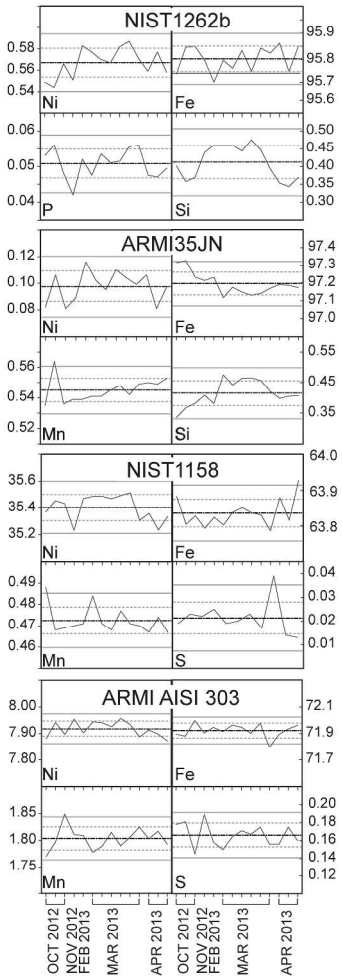

Figure 3. Temporal variations of the Ni, Fe, P, Si, Mn and S concentrations in CRMs by HHXRF over a period of six months to exemplify the long-term instrumental precision. All concentrations are % m/m. Top and bottom continuous lines on each diagram represent positive and negative 2-sigma variation range, respectively; top and bottom dotted lines on each diagram represent positive and negative 1-sigma variation range, respectively.
297x420mm (300 x 300 DPI)

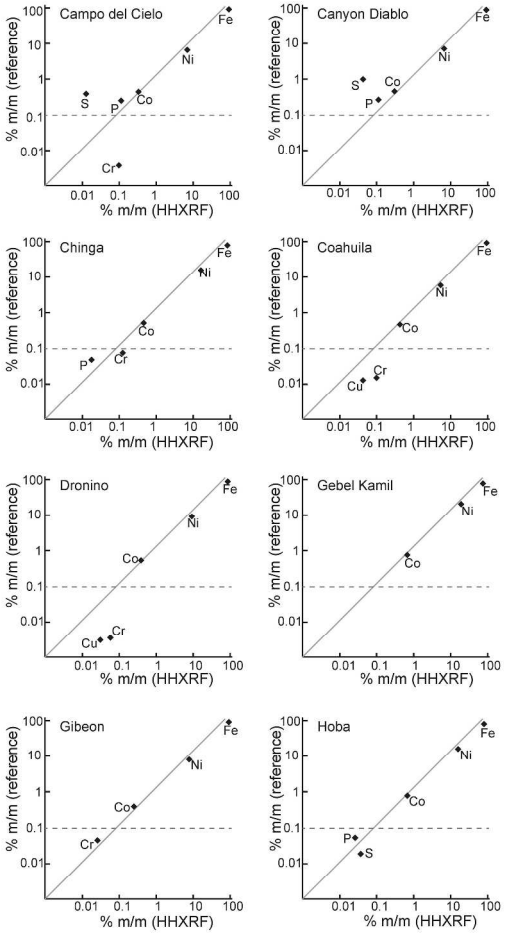

Figure 4. HHXRF elemental concentrations of iron meteorites plotted versus reference values from literature (see Table 4 for data sources). The grey line shows the 1:1 linear correlation. For some elements in concentrations below 0.1% m/m (dotted line) such as Cu and Cr there is a weak accordance between HHXRF analysis and reference data.
297x420mm (300 x 300 DPI)

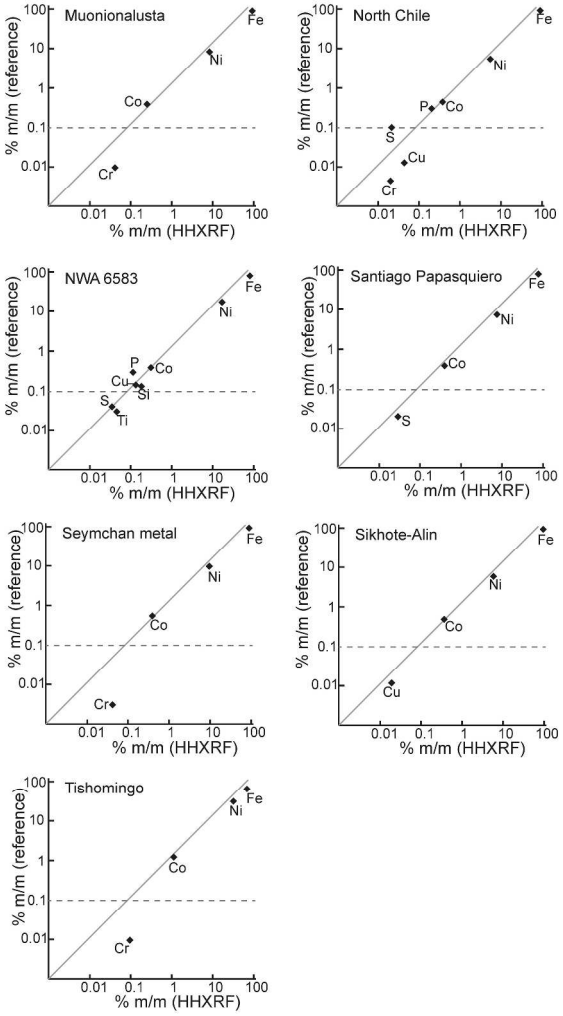

Figure 4. (continued)
297x420mm (300 x 300 DPI)

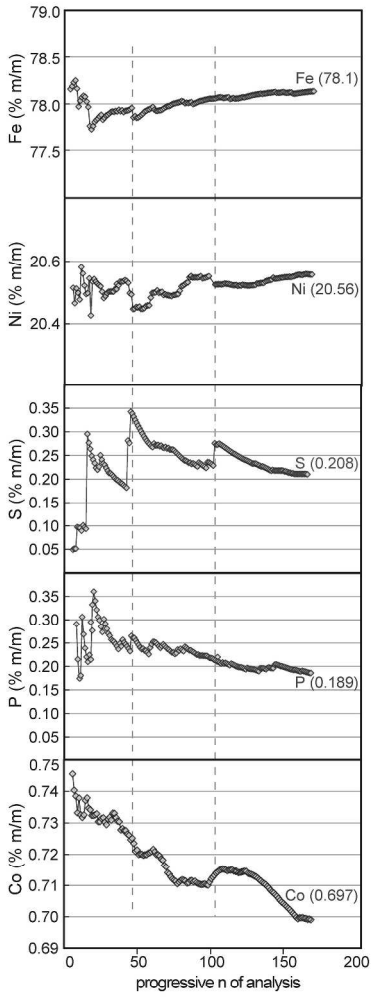

Figure 5. Dynamic average profiles of Fe, Ni, S, P and Co concentrations from 166 HHXRF spot analyses of the Gebel Kamil iron meteorite. Final average values are reported in each diagram.
297x420mm (300 x 300 DPI)

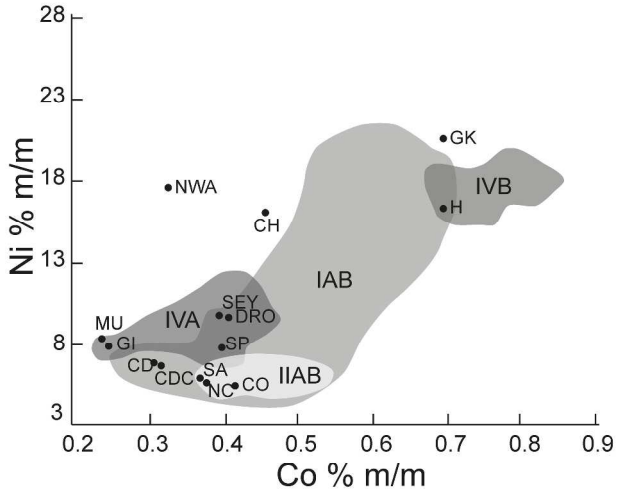

Figure 6. Ni vs. Co classification diagram for iron meteorites. Compositional fields show the ranges of iron meteorite classes from literature. The bulk metal compositions of the fourteen iron meteorites analysed by HHXRF are shown. Abbreviations: GK= Gebel Kamil; H= Hoba; CH= Chinga; NWA= NWA6583; CO= Coahuila; NC= North Chile; SP= Santiago Papasqueiro; SA= Sikhote-Alin; DRO= Dronino; SEY= Seymchan, metal; CDC= Campo del Cielo; CD= Canyon Diablo; GI= Gibeon; MU= Muonionalusta. The ungrouped meteorite Tishomingo (Ni=31.3% m/M, Co=1.3% m/m) is omitted here.
297x420mm (300 x 300 DPI)

Table 1.
NITON XL3t GOLDD+ operating conditions.

Mode	General metals
	Main (50 kV, 40 µA) - filter material: AlFe
	Al, Ti, V, Cr, Mn, Fe, Co, Ni, Cu, Zr, Nb, Mo, Sn, Sb, W
	Low (15 kV, 133 µA) - filter material: Fe
	Ti, V, Cr
	Light (8 kV, 200 µA) - no filter
	Al, Si, P, S
Counting times	Main - 60 seconds
	Low - 60 seconds
	Light - 60 seconds
	total counting time: 180 s
Spot	8 mm

Table 2.

List of analysed iron meteorites and CRMs.

Sample	Chemical classification	Structural classification*	Reference
Campo del Cielo	IAB-Main Group	Og	(Wasson and Kallemeyen 2002)
Canyon Diablo	IAB-Main Group	Og	(Wasson and Kallemeyen 2002)
Chinga	Ungrouped	D	(Buchner *et al.* 2012)
Coahuila	IIAB	H	(Wasson *et al.* 2007)
Dronino	Ungrouped	D	(Russell *et al.* 2004)
Gebel Kamil	Ungrouped	D	(D'Orazio *et al.* 2011)
Gibeon	IVA	Of	(Wasson and Richardson 2001)
Hoba	IVB	D	(Walker *et al.* 2008)
Muonionalusta	IVA	Of	(Wasson and Richardson 2001)
North Chile	IIAB	H	(Wasson *et al.* 2007)
NWA 6583	Ungrouped	D-an	(Fazio *et al.* 2013)
Santiago Papasquiero	Ungrouped	H	(Buchwald, 1975)
Seymchan	Pallasite-Main Group	Og˜	(van Niekerk *et al* . 2007)
Sikhote-Alin	IIAB	Ogg	(Wasson *et al.* 2007)
Tishomingo	Ungrouped	D	(Birch *et al.* 2001)
CRMs			
ARMI AISI 303	Austenitic stainless steel		www.armi.com
NIST-1158	High-Ni steel		www.nist.gov
NIST-1262b	Steel		www.nist.gov
ARMI 35JN	Steel		www.armi.com

*Ogg=coarsest octahedrite, Og=coarse octahedrite, Of=fine octahedrite, H=hexahedrite, D=ataxite, D-an=anomalous ataxite; ˜referred to Seymcham metal fraction.

Table 3.
HHXRF analyses on metal alloy CRMs.

		NIST1262b					ARMI 35JN					ARMI AISI303					NIST1158				
	Unit	Ref.*	Estimated uncertainty	HHXRF (n=11)	st. dev.	RSD%	Ref.**	Estimated uncertainty	HHXRF (n=11)	st. dev.	RSD%	Ref.**	Estimated uncertainty	HHXRF (n=11)	st. dev.	RSD%	Ref.*	Estimated uncertainty	HHXRF (n=11)	st. dev.	RSD%
Al	µg g^{-1}	810	20	<LOD	-	-	290	10	<LOD	-	-	-	-	-	-	-	-	-	-	-	-
Si	% m/m	0.4	0.01	0.412	0.047	11	0.6	0.01	0.415	0.042	10	0.22	0.01	0.097	0.023	29	0.194	0.003	<LOD	-	-
P	% m/m	0.044	0.001	0.048	0.005	10	0.006	0.001	<LOD	-	-	0.025	0.001	<LOD	-	-	0.003	0.001	<LOD	-	-
S	% m/m	0.037	0.001	0.036	0.007	20	0.025	0.002	<LOD	-	-	0.34	0.01	0.403	0.013	7	0.005	0.002	0.021	0.007	33
Ti	µg g^{-1}	1000	40	710	30	4	20	1	<LOD	-	-	-	-	-	-	-	-	-	-	-	-
V	µg g^{-1}	410	10	160	20	16	40	4	<LOD	-	-	1000	20	970	120	12	-	-	-	-	-
Cr	% m/m	0.3	0.01	0.3	0.06	2	1.18	0.02	1.211	0.007	1	18.24	0.03	18.07	0.042	0.2	0.063	0.008	0.123	0.007	6
Mn	% m/m	1.05	0.01	1.041	0.009	1	0.55	0.01	0.551	0.008	1	1.98	0.02	2.006	0.032	2	0.47	0.007	0.47	0.006	1
Fe	% m/m	95.3	-	95.8	0.050	0.05	97.1	-	97.2	0.1	0.1	68.7	-	69.1	0.1	0.2	63.2	-	63.8	0.04	0.1
Co	% m/m	0.3	0.01	0.189	0.051	27	-	-	-	-	-	0.208	0.002	0.242	-	-	0.008	0.002	0.058	0.058	100
Ni	% m/m	0.59	0.01	0.567	0.013	2	0.086	0.002	0.098	0.011	12	9.5	0.03	9.317	0.028	0.4	36.1	0.029	35.4	0.1	0.3
Cu	µg g^{-1}	5100	100	5790	80	1	870	20	830	40	4	5100	100	5120	120	2	400	20	740	110	15
Zr	µg g^{-1}	2200	100	1850	30	2	-	-	-	-	-	-	-	-	-	-	-	-	-	-	-
Nb	µg g^{-1}	3000	100	3120	30	1	20	10	<LOD	-	-	-	-	-	-	-	-	-	-	-	-
Mo	µg g^{-1}	700	10	660	10	2	4500	100	4590	30	1	1300	20	1320	30	1	110	20	110	3	2
Sn	µg g^{-1}	160	10	220	20	8	50	10	70	10	13	-	-	-	-	-	-	-	-	-	-
Sb	µg g^{-1}	120	10	150	10	8	20	5	<LOD	-	-	-	-	-	-	-	-	-	-	-	-
W	µg g^{-1}	2000	100	2810	40	2	30	-	<LOD	-	-	-	-	-	-	-	-	-	-	-	-

References values from *NIST certificate, **ARMI certificate.

Table 4.
HHXRF analyses of bulk metal of the studied meteorite samples. All elements in % m/m except Ti, Cr, Cu, W in µg g^{-1}

	Campo del Cielo				Canyon Diablo			
	ref.	average (n=15)	st. dev.	RSD%	*ref.*	average (n=21)	st. dev.	RSD%
Si	-	<LOD	-	-	-	<LOD	-	-
P	*0.25*	0.112	0.024	22	*0.26*	0.11	0.01	13
S	*0.4*	0.013	0.002	19	*1*	0.04	0.01	15
Ti	-	<LOD	-	-	-	<LOD	-	-
Cr	*37*	970	760	79	-	400	100	13
Fe	*92.8*	92.7	0.2	0.2	*89.8-92.4*	92.8	0.2	0.2
Co	*0.42 - 0.47*	0.32	0.02	8	*0.28*	0.31	0.01	4
Ni	*6.5 - 7.13*	6.6	0.2	3	*7.1*	6.7	0.2	2
Cu	*50*	<LOD	-	-	-	<LOD	-	-
W	*1*	510	50	9	-	<LOD	-	-

	Chinga				Coahuila			
	ref.	average (n=15)	st. dev.	RSD%	*ref.*	average (n=3)	st. dev.	RSD%
Si	-	<LOD	-	-	-	<LOD	-	-
P	*0.05*	0.018	0.002	11	-	0.128	0.006	5
S	-	0.126	0.221	173	-	<LOD	-	-
Ti	-	<LOD	-	-	-	<LOD	-	-
Cr	*810*	1220	410	33	*370*	970	50	5
Fe	*82.7-83.2*	83.3	0.2	0.2	*93.9-94.1*	93.9	0.004	0.004
Co	*0.54-0-57*	0.46	0.03	6	*0.41-0.44*	0.42	0.005	1
Ni	*16.2-16.6*	16.2	0.2	1	*5.49-5.59*	5.4	0.002	0.04
Cu	-	<LOD	-	-	*120-170*	420	30	7
W	-	<LOD	-	-	-	<LOD	-	-

	Dronino				Gebel Kamil			
	ref.	average (n=20)	st. dev.	RSD%	*ref.*	average (n=22)	st. dev.	RSD%
Si	-	<LOD	-	-	-	<LOD	-	-
P	-	0.017	0.002	13	-	0.041	0.01	27
S	-	1.2	1.2	101	-	0.023	0.07	29
Ti	-	<LOD	-	-	-	<LOD	-	-
Cr	*40*	590	400	67	-	600	300	50
Fe	*89.6*	88.7	1.4	2	*78.6*	78.5	0.2	0.3
Co	*0.55*	0.41	0.04	10	*0.76*	0.69	0.05	7
Ni	*9.8*	9.6	0.5	5	*20.6*	20.6	0.21	1
Cu	*30*	320	70	21	-	700	100	14
W	-	<LOD	-	-	-	<LOD	-	-

	Gibeon				Hoba			
	ref.	average (n=11)	st. dev.	RSD%	*ref.*	average (n=3)	st. dev.	RSD%
Si	-	<LOD	-	-	-	<LOD	-	-
P	-	0.016	0.003	22	*0.055*	0.027	0.003	10
S	-	0.095	0.031	32	*0.02*	0.038	0.038	100
Ti	-	280	150	55	-	<LOD	-	-
Cr	*130-370*	260	160	60	-	<LOD	-	-
Fe	*91.2-92.3*	91.8	0.1	0.2	*82.4-82.8*	82.9	0.1	0.2
Co	*0.37-0.39*	0.25	0.01	5	*0.74-0.79*	0.7	0.003	0.4
Ni	*7.25-8.27*	7.8	0.1	0.7	*16.4-16.8*	16.3	0.1	0.6
Cu	*140-200*	<LOD	-	-	-	<LOD	-	-
W	-	<LOD	-	-	-	<LOD	-	-

Reference values (min-max) mainly from: Buchwald 1975 (and references therein), Scott and Wasson 1976, Wlotzka and Jarosewich 1977, Jochum *et al.* 1980, Wasson and Ouyang 1990,

Choi *et al.* 1995, Wasson *et al.* 1998, Benedix *et al.* 2000, Birch *et al.* 2001, Wasson and Richardson 2001, Wasson and Kallemeyen 2002, Petaev and Jacobsen 2004, Russell *et al.* 2004, van Niekerk *et al.* 2007, Wasson *et al.* 2007, Walker *et al.* 2008, D'Orazio *et al.* 2011, Buchner *et al.* 2012, Fazio *et al* . 2013.

Table 4 (continued).

	Muonionalusta				North Chile			
	ref.	average (n=15)	st. dev.	RSD%	*ref.*	average (n=5)	st. dev.	RSD%
Si	-	<LOD	-	-	-	<LOD	-	-
P	-	0.04	0.03	9	*0.3*	0.21	0.08	4
S	-	<LOD	-	-	*0.1*	0.022	0.006	3
Ti	-	<LOD	-	-	-	<LOD	-	-
Cr	*100*	400	300	61	*50*	210	170	8
Fe	*90.7-91.4*	91.3	0.04	0.05	*93.4-93.7*	93.7	0.2	0.03
Co	*0.39-0.41*	0.24	0.01	5	*0.21*	0.381	0.013	0.3
Ni	*8.2-8.9*	8.3	0.05	1	*5.6-5.7*	5.6	0.2	0.3
Cu	*110*	<LOD	-	-	*130*	450	40	0.8
W	-	<LOD	-	-	-	<LOD	-	-

	NWA 6583				Santiago Papasquiero			
	ref.	average (n=6)	st. dev.	RSD%	*ref.*	average (n=4)	st. dev.	RSD%
Si	*0.13*	0.19	0.11	56	-	<LOD	-	-
P	*0.3*	0.119	0.073	62	*0.01*	<LOD	-	-
S	*0.04*	0.037	0.016	42	*0.022*	0.030	0.003	11
Ti	*300*	470	140	29	-	-	-	-
Cr	-	0.06	0.03	44	-	-	-	-
Fe	*81.8*	81.7	0.2	0.2	*92.08*	91.7	0.106	0.115
Co	*0.39*	0.33	0.03	10	*0.38*	0.395	0.009	2.3
Ni	*17.7*	17.5	0.1	0.42	*7.51*	7.71	0.031	0.407
Cu	*1400*	1410	210	15	-	-	-	-
W	-	<LOD	-	-	-	-	-	-

	Seymchan metal				Sikhote-Alin			
	ref.	average (n=15)	st. dev.	RSD%	*ref.*	average (n=10)	st. dev.	RSD%
Si	-	<LOD	-	-	-	<LOD	-	-
P	-	0.067	0.025	37	-	0.184	0.021	11
S	-	0.033	0.019	57	-	0.031	0.01	33
Ti	-	<LOD	-	-	-	<LOD	-	-
Cr	*30*	410	350	84	-	<LOD	-	-
Fe	*90.1*	89.8	0.3	0.4	*93.6-93.8*	93.2	0.5	1
Co	*0.53*	0.4	0.02	4	*0.47-0.51*	0.37	0.06	16
Ni	*9.3*	9.7	0.3	4	*5.7-5.87*	5.8	0.3	4
Cu	-	<LOD	-	-	*130-190*	190	20	11
W	-	<LOD	-	-	-	140	10	7

	Tishomingo			
	ref.	average (n=3)	st. dev.	RSD%
Si	-	<LOD	-	-
P	-	<LOD	-	-
S	-	0.034	0.015	45
Ti	-	<LOD	-	-
Cr	*100*	940	110	11
Fe	*66.7*	67.1	0.3	0.4
Co	*1.26*	1.13	0.01	1
Ni	*32.1*	31.3	0.3	1
Cu	-	<LOD	-	-
W	-	<LOD	-	-

Table 5.
HHXRF average limits of detection (µg g^{-1}) for the elements determined in the studied iron meteorites. Limits of detection for Fe, Ni and Co are not reported here as the concentrations of these elements are orders of magnitude higher.

Element	
W	140
Cu	340
Cr	60
Ti	40
S	210
P	200
Si	500

Limit of detection is calculated as three times the standard deviation of the concentration measured in samples with none or only a trace amount of the analyte.

Table 6.

HHXRF bulk metal and bulk meteorite (i.e. metal phase plus accessory minerals) compositions from flat, roughly polished interior surfaces of Gebel Kamil and of its external surface.

Element	Bulk metal	Bulk meteorite	External surface
Fe	78.5	78.1	66.7 - 67.9
Ni	20.6	20.6	19.2 - 23.3
Co	0.69	0.70	0.87 - 1.05
P	0.04	0.19	0.06 - 0.09
S	0.02	0.21	1.35 - 1.85
Cr	0.06	0.09	0.03 - 0.05
Cu	0.07	0.06	0.07 - 0.10
Al	-	-	1.85 - 3.80
Si	-	-	3.48 - 9.10

All values in % m/m.